Mathematical Models and Methods in Applied Sciences © World Scientific Publishing Company

Coupling compartmental models with Markov chains and measure evolution equations to capture virus mutability

Ryan Weightman

 $\label{lem:prop:condition} Department \ of \ Mathematical \ Sciences \ and \ Center \ for \ Computational \ and \ Integrative \ Biology, \\ Rutgers \ University-Camden. \\ ryanj.weightman@gmail.com$

Anthony Sbarra

 $Department\ of\ Mathematical\ Sciences,\ Rutgers\ University\text{-}Camden.$ ajs686@scarletmail.rutgers.edu

Benedetto Piccoli

The COVID-19 pandemic lit a fire under researchers who have subsequently raced to build models which capture various physical aspects of both the biology of the virus and its mobility throughout the human population. These models could include characteristics such as different genders, ages, frequency of interactions, mutation of virus etc. Here we propose two mathematical formulations to include virus mutation dynamics. The first uses a compartmental epidemiological model coupled with a discrete-time finite-state Markov chain. If one includes a nonlinear dependence of the transition matrix on current infected, the model is able to reproduce pandemic waves due to different variants. The second approach expands such an idea to a continuous state-space leveraging a combination of ordinary differential equations with an evolution equation for measure. This approach allows to include reinfections with partial immunity with respect to variants genetically similar to that of first infection.

Keywords: epidemiology; SARS-CoV-2; SIRS compartmental models; measure differential equations; measure theory

1. Introduction

Throughout the COVID-19 pandemic there has been a growing need for more robust predictive epidemiological models in order to help policy makers answer important questions about the future ^{4,48}. Policy decisions must balance the prevention of morbidity and mortality with the preservation of societal functioning ¹⁹. Researchers work to answer questions such as: what sort of non-pharmaceutical interventions

will still be important to a population during and after a vaccination campaign 5,43 ? How do age and physical space affect the dynamics of a virus 6,29,13,18 ? What do the variables associated with the virus depend upon, and can such variables be made more dynamic to better understand long term viral propagation through a population 2,3,10,47 ?

As COVID-19 moves towards a possible endemic stage, including a method which can capture mutation is imperative to more long term predictions ^{30,26}. Such methods could be useful when modeling endemic response to many viruses, such as response to the seasonal flu ^{15,12,21}. Understanding the dynamics of a changing system helps in directing public response against a virus ^{40,16,36}. It takes multiple months for a government to identify, address and release policy to mitigate the risk of a new disease ^{27,46}. It then takes the public time to react and begin following such policies ³⁷. The ability to model a changing virus could vastly cut down on decision making time and thus help a society react more efficiently.

Here we introduce two methodologies to consider mutation of a virus. We first assume a discrete-time process where the virus mutates from variant A to variant B at fixed intervals of time. Mathematically, this amounts to coupling a classical epidemiological model based on ordinary differential equations, with a discrete-time Markov chain. The latter contains a finite set of states, corresponding to the major variants of interest. We focus on the classical SIRS model (Susceptible-Infected-Removed-Susceptible). The model properties are immediate from the discrete-time properties of the Markov chain, including positivity of solutions and conservation of mass. Then, we propose a nonlinear transition matrix, to take into account the effect of the total number of infected over the virus mutability. This modification allows to reproduce various pandemic waves linked to different mutations, see Section 2.3.

Our second model proposes a continuous diffusion process for virus variants, where the infection begins somewhere on a continuous state-space of possible variants and, as time progresses, the virus diffuses over the same space. We choose a measure-theoretic approach proposed in 44 called measure differential equations (briefly MDEs). Such framework is very general and flexible, allowing to couple ordinary differential equations (briefly ODEs), e.g. for susceptible population, with measure evolution equations, or for infected differentiated by the virus variant. In particular, a first model coupling ODEs and MDEs was proposed in ²⁵ with results on existence and uniqueness of trajectories. Here, we extend this model to include reinfection. The latter is modelled by an additional compartment, called recovered susceptible. In this compartment, individuals have partial immunity to variants genetically similar to that of the first infection. This is realized by an infection rate that depends both on the original variant and the new infecting variants. We prove that this extended model can be cast within the general theory developed in ²⁵. Then, we focus on simulations, using a scheme combining numerical approximations for ODEs and lattice approximate solutions for MDEs. The latter is based on approximating measure with finite sums of Dirac deltas centered at the points of a lattice. The simulations show how the model can track the variants dynamics together with the many compartments. The resulting dynamics shows a rich set of possible evolution. Concluding, these new approaches bring us closer to developing tools for pandemic management.

The focus of this paper is in introducing two mathematical formulations to include mutation dynamics of a virus, and is organized as follows. First we introduce epidemiological models in a general sense in Section 1.1. We then define our first model, an MC-ODE system which uses a discrete-time finite-state MC to govern mutation dynamics. In Section 2 we define the properties of this system before presenting simulations of a theoretical model built in Matlab using variables inspired by the COVID-19 pandemic. In Section 3 we introduce MDEs and define the characteristics of such equations. We then describe the general theory for coupled ODE-MDE systems in Section 4. Using such a formulation, in Section 5, we generalize our model to a continuous state-space by introducing a measure for the mutation space, rather than a vector of variants. We define the coupled system and provide a method for solving the system. We then introduce properties of the system of equations before providing simulations, once again, of a theoretical model built in Matlab using variables inspired by the COVID-19 pandemic.

1.1. Epidemiological modeling

Epidemiological models come in two general forms: agent based and compartmental ¹⁵. The more popular models tend to be compartmental as they have a lower computational cost associated with larger population sizes and remove stochasticity thus leaving space for predictions based on optimal control ^{33,39,41}. The models are designed using population compartments, which sum together at any given time to be the total population. Models that are proposed here are an expansion of SIR models ³². These classical models are built using three compartments: susceptible, infectious, and removed with the following general structure: $\dot{S} = -\frac{\beta SI}{N}$, $\dot{I} = \frac{\beta SI}{N} - \gamma I$, $\dot{R} = \gamma I$, where β and γ are the infection rate and recovery rate respectively. The infection rate and recovery rate combine to form what we call the "replication rate" represented by R_0 where $R_0 = \frac{\beta}{\gamma}$. The replication rate of a virus, or basic reproduction number, is the leading driver in prediction and works as follows: A variant with a replication rate of 2 means that for each person infected, they will infect two others. A replication rate under 1 would mean that for each person infected, they are infecting less than one person, thus the virus is diminishing ³⁵. A benefit of such a model is the ability to scale compartments to fit the needs of the researcher, such as capturing disease progression ^{23,24}, considering age structure and spacial distance ^{14,11,52,52}, and even projecting the need for hospital beds as the virus progresses ¹.

2. Markov chain coupled with ODEs

2.1. Motivation and definition of MC-ODE system

From August 2020 until December 2020, the Beta variant of SARS-CoV-2 was dominant. Later, from December 2020 until April 2021, the Alpha variant took stage.

The Gamma variant began to become more prevalent, only to be outpaced by the Delta variant before having a chance to become dominant ^{8,49}. Lastly, the Omicron variant appeared in November 2021 and held its position as the lead infection holder through the new year ^{22,31}. With each new dominant variant, a new set of defining parameters are required for predictive modeling ^{51,42}. With a seemingly discrete number of dominant variants, one may choose to model the interactions and mutations in a discrete way ⁹. We use a SIR model coupled with a nonlinear discrete-time Markov chain (briefly NDMC) representing the emergence of virus variants. The system will be fully coupled, but the discrete-time nature of the Markov chain allows a simple mathematical treatment and simulations.

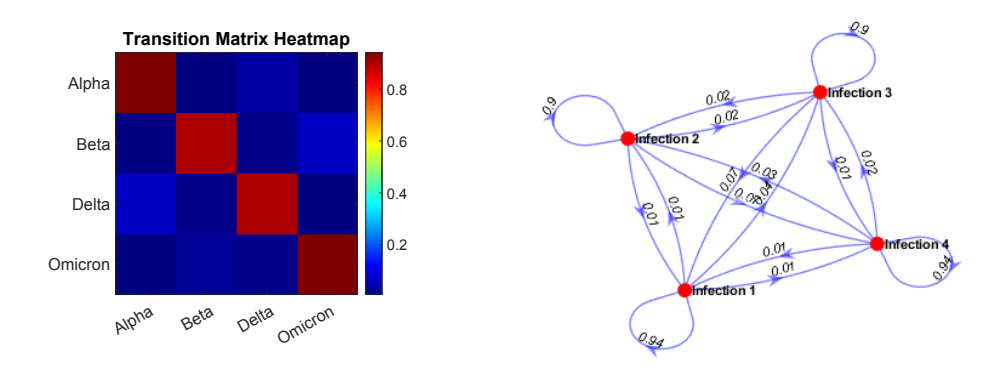


Fig. 1: Left: heatmap representing the transition matrix. Right: graph representation of the Markov chain with main COVID-19 variants.

Assume the infected population is represented by a sequence of random variables $I_i:\Omega\to\mathcal{I}$, with (Ω,\mathcal{F},P) measure space and $\mathcal{I}=\{I^1,\ldots,I^p\}$ representing the distribution over the space representing the set of significant virus mutations. The meaning is the following: the total population of infected people $\sum_i I_i$ will follow a standard compartmental model, with $I_i/\sum_i I_i$ representing the probability of the generic infected person to have variant i. Alternatively, we can think of \mathcal{I} as a vector representing the infected population distinguished in sub-populations via the virus variants. We assume that the evolution of \mathcal{I} is given by a NDMC associated to a transition matrix $T = \{t(i,j)\}_{i,j=1,\ldots,p}$. An example of NDMC using the COVID-19 main variants is given in Figure 1. The goal is then to use the discrete-time evolution of the MC for infected distribution with time-varying mass coupled with the SIR dynamics. Assuming the time step of the Markov chain is given by Δt , the coupled

ODE-MC dynamics is given by:

$$\begin{cases} \dot{S} = -\sum_{i=1}^{p} \beta_{i} \frac{S(t)}{N} I_{i}(t) + \sigma_{i} R(t), \\ \dot{I}_{i} = \beta_{i} \frac{S(t)}{N} I_{i}(t) - \gamma_{i} I_{i}(t), \\ \dot{R} = \sum_{i=1}^{p} \gamma_{i} I_{i}(t) - \sigma_{i} R(t), \end{cases}$$

$$(2.1)$$

$$\mathcal{I}(k\Delta t +) = \mathcal{I}(k\Delta t) \cdot T(\mathcal{I}(k\Delta t)), \ k \in \mathbb{N}.$$

Here S is the susceptible population, $I_i(t)$ is the population infected by the i-th variant, R recovered population, N the total population, β_i , γ_i , σ_i , respectively represent the infection rate, recovery rate, and loss of immunity rate, of the ith variant. Notice that the Markov chain term $\mathcal{I}^+(k\Delta) = \mathcal{I} \cdot T(\mathcal{I})$ redistributes the infected population among the different variants every Δt time units. $T(\mathcal{I})$ represents a transition matrix for the Markov chain which governs the mutations, and the dependence on \mathcal{I} makes it a nonlinear MC. The state of this MC is a dynamic characteristic tied to both the number of infected people with the given variant and the total infected. In the simulations to follow, we choose $T_{ii}(\mathcal{I}) = T_{ii} \cdot \psi(I_i)$, where $\psi(I_i) = 1 - \eta[I_i - \bar{I}_i]_+$. Here, \bar{I}_i is a chosen threshold and η depends on both the total infected and amount of infected with infection i. Clearly in a discrete state space, the transition matrix would be MxM where M represents the number of infectious variants. In a continuous state space our equations would need to account for a continuous spectrum of variants which will be addressed in the next section. The presence of the Markov chain term is the key difference between our model and the usual SIR, allowing for the mutation of infected populations seen strongly in the wide field of variants of Sars-CoV-2. Using the above described equations, a Markov chain coupled SIR model is able to simulate the dynamics of a virus spreading through a population while capturing the changing characteristics of the disease due to new variants appearing and taking hold over the majority of the field of infections.

2.2. Properties of MC-ODE system

For system (2.1), S and R evolve continuously in time, while the infected populations I_i jump at times $k\Delta t$. A solutions is defined as follows.

Definition 2.1. A solution to (2.1) is a triple $(S, \mathcal{I}, R) : [0, T] \to \mathbb{R} \times \mathbb{R}^p \times R$ such that the following holds.

• The maps $t \to S(t)$ and $t \to R(t)$ are absolutely continuous and satisfy $(2.1)_{1,3}$ for almost every time t;

- The map $t \to \mathcal{I}$ is absolutely continuous in time on $\mathbb{R} \setminus \{k\Delta t : k \in \mathbb{N}\}$, with components I_i satisfying $(2.1)_{1,3}$ for almost every time $t \in \mathbb{R} \setminus \{k\Delta t : k \in \mathbb{N}\}$:
- At times $\{k\Delta t : k \in \mathbb{N}\}\ \mathcal{I}$ is right-continuous and satisfy $(2.1)_4$.

One can easily prove the following:

Lemma 2.1 (Positivity). Consider a solution to (2.1) with $S(0) \ge 0$, $I_i(0) \ge 0$, i = 1, ..., p, $R(0) \ge 0$, then $S(t) \ge 0$, $I_i(t) \ge 0$, i = 1, ..., p, $R(t) \ge 0$ for every t > 0 and $N(t) = S(t) + \sum_{i=1}^{p} I_i + R(t)$ is contant in time.

2.3. Simulations for Markov chain model

There have been four dominant variants throughout the COVID-19 pandemic (up to early 2022), thus we focus on them for our definitions of parameters. It is worth noting that the model is adaptable to any number of variants as long as computational cost is considered. All infection rates and recovery rates in this section are determined by the specific characteristics of the variants of COVID-19, with data found in related literature 50,38 . Specifically, the following estimated replication rates were used: 2.1, 1.95, 3.15, 3.16 for the variants Alpha, Beta, Delta, and Omicron, respectively. For simulations that include reinfection, we consider a 60 day immunity followed by returning to the susceptible population. The recovery rate, or γ , is set to a constant 14 days from infection.

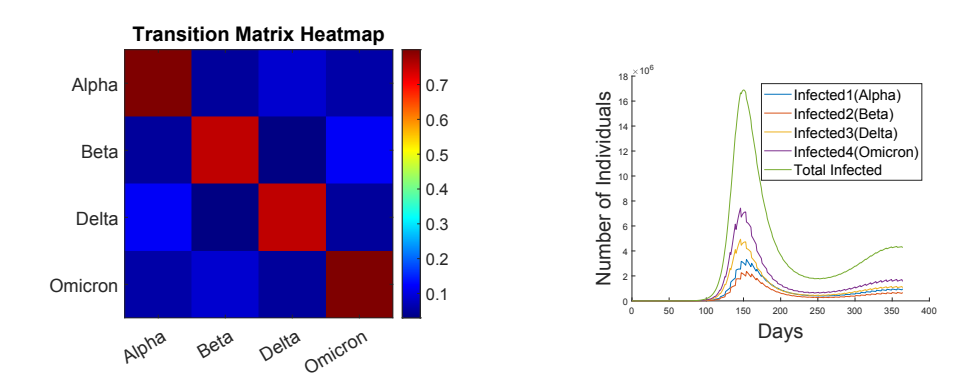
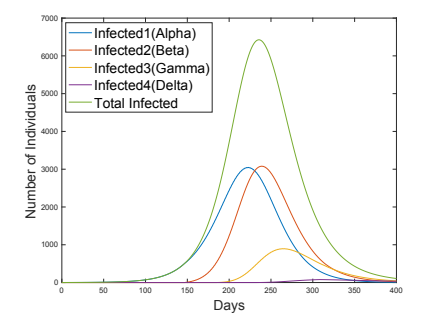


Fig. 2: Static Markov chain example

In Figure 2 we illustrate a simple example of a linear transition matrix (not dependent on the infected population \mathcal{I} , thus corresponding to a linear MC. We notice that such models let all the variants peak at the same time, something which did not happen for COVID-19. Therefore, we consider the case of nonlinear MC, with $T_{ii}(\mathcal{I}) = \tilde{T}_{ii} \cdot \psi(I_i)$, where $\psi(I_i) = 1 - \eta_i [I_i - \bar{I}_i]_+$. In our simulations, we choose $\eta_i = .005 * \frac{I(i)}{I \mathcal{I}}$ and $\bar{I}_i = 300$. The corresponding dynamics is depicted in Figure



Infected1(Alpha) Infected3(Gamma Infected4(Delta)

Fig. 3: Evolution for nonlinear MC without reinfection.

Fig. 4: Evolution for nonlinear MC with reinfection.

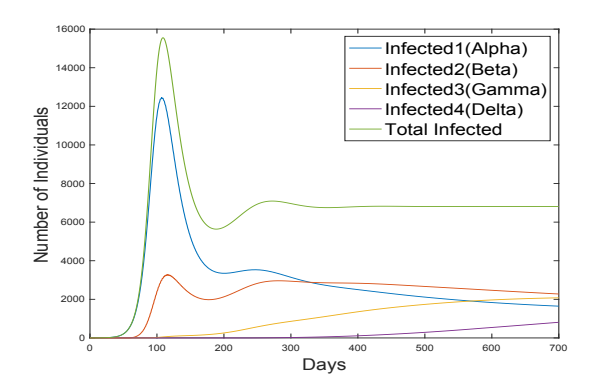


Fig. 5: Evolution for replication rate $R_0 = 2.5$ across all variants.

3 for a simulation corresponding to 400 days. We notice that the virus mutates slowly at the start as the first infection takes hold. As the total infected grows, the mutability increases, giving rise to other variants. Infection four in this simulation, despite having the largest infection rate, never takes hold as the dominant variant due to a lack of reinfection. This highlights the importance of modeling reinfection, which is done in Figure 4. Here, one can appreciate the drastic difference between the long term predictions of Figures 3 and 4. In 4, infection four is the last to take hold and in fact will become endemic having the highest infection rate. Lastly, we run the same model but with all replication rates $R_0 = \frac{\beta_i}{\gamma_i}$ equal to 2.5, see Figure 5. Trajectories are very different from the data observed during the COVID-19 pandemic. This discrepancy is due to the general notion that a virus mutates towards more aggressive variants, as shown in their heightened infection rates, as an evolutionary trajectory.

3. Measure differential equations with source

We recall the main definitions and properties of MDEs, first introduced in ⁴⁴, then further developed and analyzed in ⁷ and extended to include sources in ⁴⁵.

The definition of MDE is a natural generalization of Ordinary Differential Equation and based on the concept of measure vector field and source. Given a Polish space X, $\mathcal{M}(X)$ indicates the space of Radon measures with finite mass on X.

Definition 3.1. A Measure Vector Field (briefly PVF) is a map $V: \mathcal{M}(\mathbb{R}^n) \to \mathcal{M}(T\mathbb{R}^n)$ such that $\pi_1 \# V[\mu] = \mu$, where $\pi_1 : T\mathbb{R}^n \to \mathbb{R}^n$ is the canonical projection. A source is a map $h: \mathcal{M}(\mathbb{R}^n) \to \mathcal{M}(\mathbb{R}^n)$.

A Measure Differential Equation with MVF V and source h is defined by:

$$\dot{\mu} = V[\mu] \oplus h[\mu],\tag{3.1}$$

and a solution to (3.1) is a map $\mu:[0,T]\to\mathcal{M}(\mathbb{R}^n)$ such that the following holds. For every $f\in\mathcal{C}_c^\infty(\mathbb{R}^n)$, the integral $\int_{T\mathbb{R}^n}(\nabla f(x)\cdot v)\ dV[\mu(s)](x,v)$ is defined for almost every $s,\ s\to\int_{T\mathbb{R}^n}(\nabla f(x)\cdot v)\ dV[\mu(s)](x,v)\in L^1([0,T]),\ t\to\int f\ d\mu(t)$ is absolutely continuous and

$$\frac{d}{dt} \int_{\mathbb{R}^n} f(x) \, d\mu(t)(x) = \int_{T\mathbb{R}^n} (\nabla f(x) \cdot v) \, dV[\mu(t)](x, v) + \int_{\mathbb{R}^n} f(x) dh[\mu(t)](x), \quad (3.2)$$

holds for almost every $t \in [0, T]$. In simple words, the MVF V spread the mass of μ along the directions in the fiber components, while the source h adds or subtracts mass.

Existence of solutions to (3.1) is guaranteed under natural assumptions. To state such assumptions, we need to recall the definition of generalized Wasserstein distance:

Definition 3.2 (The generalized Wasserstein distance). Let $\mu, \nu \in \mathcal{M}(X)$ be two measures. We define the functional

$$W^{g}(\mu,\nu) := \inf_{\tilde{\mu},\tilde{\nu} \in \mathcal{M}, |\tilde{\mu}| = |\tilde{\nu}|} |\mu - \tilde{\mu}| + |\nu - \tilde{\nu}| + W(\tilde{\mu},\tilde{\nu}). \tag{3.3}$$

It is easy to check that the infimum is achieved by a couple $(\tilde{\mu}, \tilde{\nu})$ such that $\tilde{\mu} \leq \mu$ and $\tilde{\nu} \leq \nu$. We also introduce the operator \mathcal{W}^g . Fix $V_1, V_2 \in \mathcal{M}(T\mathbb{R}^n)$, and define $\mathcal{V}(V_1, V_2)$ to be the set of pairs $(\tilde{V}_1, \tilde{V}_2)$, such that $\tilde{V}_i \leq V_i$, i = 1, 2, and $W^g(\mu_1, \mu_2) = |\mu_1 - \tilde{\mu}_1| + W(\tilde{\mu}_1, \tilde{\mu}_2) + |\mu_2 - \tilde{\mu}_2|$, where $\mu_i = \pi_1 \# V_i$ and $\mu_i = \pi_1 \# V_i$, i = 1, 2. We also denote by $P(\tilde{V}_1, \tilde{V}_2)$ the set of transference plans between V_1 and V_2 and by $P^{opt}(\tilde{\mu}_1, \tilde{\mu}_2)$ the set of optimal transference plans between $\tilde{\mu}_1$ and $\tilde{\mu}_2$. We set

$$\mathcal{W}^{g}(V_{1}, V_{2}) = \inf \left\{ \int_{T\mathbb{R}^{n} \times T\mathbb{R}^{n}} |v - w| \, dT(x, v, y, w) : \right.$$

$$T \in P(\tilde{V}_{1}, \tilde{V}_{2}), (\tilde{V}_{1}, \tilde{V}_{2}) \in \mathcal{V}(V_{1}, V_{2}), \pi_{13} \# T \in P^{opt}(\tilde{\mu}_{1}, \tilde{\mu}_{2}), \right\}, \tag{3.4}$$

(H1) V is support sublinear, i.e. there exists C > 0 such that for every $\mu \in \mathcal{M}(X)$ it holds:

$$\sup_{(x,v)\in Supp(V[\mu])} |v| \le C \left(1 + \sup_{x\in Supp(\mu)} |x|\right).$$

(H2) the map $V: \mathcal{M}(\mathbb{R}^n) \to \mathcal{M}(T\mathbb{R}^n)$ satisfies:

$$W^g(V[\mu], V[\nu]) \le KW^g(\mu, \nu),$$

with K > 0 bounded for measures with uniformly bounded support.

(H3) the map h is uniformly bounded, for measures with uniformly bounded support, and Lipschitz continuous (for the topology given by the generalized Wasserstein distances W^g on \mathbb{R}^n and $T\mathbb{R}^n$).

We refer the reader to ⁴⁵ for details.

Solutions can be constructed via Lattice Approximate Solutions (briefly LAS). In simple words, LAS consist of approximating measures with finite sums of Dirac deltas centered at points of a lattice, e.g. \mathbb{Z}^n .

More precisely, fix a time-step $\Delta_N = \frac{1}{N}$, define the velocity step $\Delta_N^v = \frac{1}{N}$, the space step $\Delta_N^x = \Delta_N^v \Delta_N = \frac{1}{N^2}$ and set

$$\mathcal{A}_N^x(\mu) = \sum_i m_i^x(\mu) \delta_{x_i} \tag{3.5}$$

with $m_i^x(\mu) = \mu(x_i + Q), Q = ([0, \frac{1}{N^2}])^n$ and

$$\mathcal{A}_{N}^{v}(V[\mu]) = \sum_{i} \sum_{j} m_{ij}^{v}(V[\mu]) \ \delta_{(x_{i},v_{j})}$$
(3.6)

where $m_{ij}^v(V[\mu]) = V[\mu](\{(x_i, v) : v \in v_j + Q'\})$, and $Q' = ([0, \frac{1}{N}])^n$. The definition of LAS is as follows:

Definition 3.3. Given a MVF V, T > 0 and $N \in \mathbb{N}$, the LAS $\mu^N : [0, T] \to \mathcal{P}_c(\mathbb{R}^n)$ is defined as follows: $\mu_0^N = \mathcal{A}_N^x(\mu_0)$ and:

$$\mu_{\ell+1}^{N} = \mu^{N}((\ell+1)\Delta_{N}) = \sum_{i} \sum_{j} m_{ij}^{v}(V[\mu^{N}(\ell\Delta_{N})]) \ \delta_{x_{i}+\Delta_{N} \ v_{j}}.$$
 (3.7)

Notice that $Supp(\mu_{\ell}^{N})$ is contained in the set $\mathbb{Z}^{n}/(N^{2}) \cap [-N,N]^{n}$, thus $\mu_{\ell}^{N} = \sum_{i} m_{i}^{N,\ell} \delta_{x_{i}}$ for some $m_{i}^{N,\ell} \geq 0$. Then μ^{N} can be defined for all times by interpolation:

$$\mu^{N}(\ell \Delta_{N} + t) = \sum_{ij} m_{ij}^{v}(V[\mu^{N}(\ell \Delta_{N})]) \, \delta_{x_{i} + t \, v_{j}}.$$
(3.8)

4. General theory for coupled ODE-MDE

Here we recall the theory for coupled systems of ODEs and MDEs developed in ²⁵. A coupled ODE-MDE system is written as:

$$\begin{cases} \dot{x} = g(x, \mu) \\ \\ \dot{\mu} = V[\mu] \oplus s(\mu, x) \end{cases}$$

$$(4.1)$$

where $g: \mathbb{R}^m \times \mathcal{M}(\mathbb{R}^n) \to \mathbb{R}^m$, V is a MVF and s is a source term depending on x. In simple words, a solution to (4.1) is a couple $(x(\cdot), \mu(\cdot))$ so that x is a solution of the ODE with $t \to \mu(t)$ plugged into the right-hand side, and μ solves the MDE with $t \to x(t)$ plugged in the source term. The precise definition is as follows:

Definition 4.1. A solution to (4.1) is a couple (x, μ) , with $x : [0, T] \to \mathbb{R}^m$ and $\mu : [0, T] \to \mathcal{M}(\mathbb{R}^n)$ such that:

- 1) $t \to x(t)$ is absolutely continuous and $x(t) = x_0 + \int_0^t g(x(\tau), \mu(\tau)) d\tau$ for almost every $t \in [0, T]$.
- 2) $t \to \mu(t)$ has uniformly bounded mass, $\int_{T\mathbb{R}^n} (\nabla f(y) \cdot v) \, dV[\mu(t)](y,v)$ is defined for almost every $t \in [0,T]$, $t \to \int_{\mathbb{R}^n} f(y) \, ds[\mu(t),x(t)](y) \in L^1([0,T])$, $t \to \int_{\mathbb{R}^n} f(y) \, d\mu(t)(y)$ is absolutely continuous and for almost every $t \in [0,T]$ it satisfies:

$$\frac{d}{dt} \int_{\mathbb{R}^n} f \, d\mu(t) = \int_{T\mathbb{R}^n} (\nabla f \cdot v) \, dV[\mu(t)] + \int_{\mathbb{R}^n} f \, ds[\mu(t), x(t)]. \tag{4.2}$$

The existence of a semigroup of solutions for the system (4.1) is provided by the following theorem:

Theorem 4.1. ²⁵ Consider the system (4.1), with g locally Lipschitz uniformly in μ , the MVF V satisfying (H1), (H2), s with uniformly bounded mass and support, and satisfying for some M > 0:

$$W^{g}(s[\mu, x], s[\nu, y]) \le M(|x - y| + W^{g}(\mu, \nu)). \tag{4.3}$$

Then there exists a Lipschitz semigroup of solutions to (4.1).

5. An MDE-ODE compartmental model with virus variants dynamics

After SARS-CoV-2 infection is transmitted, the virus begins multiplying quickly. Within days, billions of virus particles have been produced, and during each replication cycle it is known that small copy mistakes occur. With about 30,000 nucleotides in the SARS-CoV-2 genome, and with each nucleotide either being adenine, cytosine, guanine, or thymine, there a fixed number of possible viral mutations of the genome. As a result, within days of the virus entering the system, so many mutations have occurred that there is a high probability that a single infected body

contains every possible genomic mutation of the virus ³⁴. Despite this maximally diverse population of mutations, the dominant strain of a previous host is extremely likely to be the dominant strain of the new host, as it is the strain which has the most time to develop a large viral load. This suggests that due to the fairly continuous process of mistakes being made and having some probability to cause a new variant, a new variant of concern could appear at any time, changing the parameters of all predictive models by invalidating the parameters of the previous dominant variant. Such realities demand the need for a more continuous mindset, where the underlying assumption is that over time the virus will mutate often and mutate to new strains not previously observed. Here we introduce an MDE inspired model for viral infections where mutations are occurring as viral dynamics in a continuous state-space.

We assume that the population of infected is represented by a measure over a space representing virus mutations. For simplicity, we parameterize these mutations using one parameter $\alpha \in \mathbb{R}$, but our framework allows for other choices. The infected population can be thought of as a continuous distribution over a closed interval. As for standard compartmental models, the population of susceptible can be identified as a single scalar value, thus $S \in \mathbb{R}$. The dynamics of the susceptible population is captured by the ODE:

$$\dot{S} = -\frac{S}{N} \int_{\mathbb{R}} \beta(\alpha) \ dI(\alpha),$$

where $\beta(\alpha)$ is the infectivity rate which now depends on the virus mutation identified by the parameter α . Before introducing the dynamics of infected population, we recall an MDE model with finite diffusion.

5.1. An MDE modeling finite speed diffusion

The MDE framework allows modeling diffusion with finite speed, which we will use for virus variants dynamics. The diffusion speed can be regulated by assigning an increasing map $\varphi:[0,1]\to\mathbb{R}$ and defining and MVF V_{φ} as follows. First we set

$$J_{\varphi}(x) = \begin{cases} \delta_{\varphi(F_{\mu}(x))} & \text{if } F_{\mu}(x^{-}) = F_{\mu}(x), \\ \frac{\varphi \# \left(\chi_{[F_{\mu}(x^{-}), F_{\mu}(x)]} \lambda\right)}{F_{\mu}(x) - F_{\mu}(x^{-})} & \text{otherwise,} \end{cases}$$

$$(5.1)$$

where $F_{\mu}(x) = \mu(]-\infty, x]$ is the cumulative distribution of μ , and λ is the Lebesgue measure. We set

$$V_{\varphi}[\mu] = \mu \otimes_x J_{\varphi}(x), \tag{5.2}$$

thus the mass at x moves with speed $\varphi(i(F_{\mu}(x)))$. For example, choosing $\varphi(\alpha)$ $\alpha - \frac{1}{2}$, the solution starting from a Dirac delta centered at 0 is given by $\mu(t) =$ $\frac{1}{t}\chi_{\left[-\frac{t}{2},\frac{t}{2}\right]}d\lambda.$

5.2. MDE-ODE system with reinfection

We now define a generalization of the example of Section 5.1 to be applied to the measure with time-varying mass I(t). First set $F_I(x) = \frac{I(]-\infty,x])}{I(\mathbb{R})}$, which is the normalized cumulative distribution of infected up to a given x value, so that $F_I(-\infty) = 0$ and $F_I(+\infty) = 1$. Fix an increasing map $\varphi : [0,1] \to \mathbb{R}$ and define $V_{\varphi}[I] = I \otimes_x J_{\varphi}(x)$, where $J_{\varphi}(x)$ is given by (5.1). The dynamics for I are given by the MDE:

$$\dot{I} = V_{\varphi}[I] + \frac{S}{N}\beta(\alpha)I - \gamma(\alpha)I$$

where $\gamma(\alpha)$ is the recovery rate, also dependent on the virus mutation. $V_{\varphi}[I]$ denotes the MVF representing the finite speed diffusion. Put simply, $V_{\varphi}[I]$ moves the ordered masses with speed prescribed by φ .

Finally a second ODE describes the dynamics of R:

$$\dot{R} = \int_{\mathbb{R}} \gamma(\alpha) \ dI(\alpha).$$

The overall dynamics consists of coupled ODEs and MDE:

$$\begin{cases} \dot{S} = -\frac{S}{N} \int_{\mathbb{R}} \beta(\alpha) \ dI(\alpha), \\ \dot{I} = V_{\varphi}[I(\alpha)] + \frac{S}{N} \beta(\alpha) I(\alpha) - \gamma(\alpha) I(\alpha), \\ \dot{R} = \int_{\mathbb{R}} \gamma(\alpha) \ dI(\alpha). \end{cases}$$
 (5.3)

A long-term effect of the pandemic is the possibility of reinfection, especially for an individual previously exposed to variants which are genetically significantly different. Modeling reinfections fits two purposes: not only to better represent the actual dynamics of COVID-19, but also to illustrate the ease with which new compartments can be added to such a system. In order to do so, we parameterize the recovered population by the same variant space as the infectious. After a certain amount of time σ , an individual becomes again vulnerable to the virus, but with some immunity with respect to the variant of original infection as well as similar variants. This reinfection is achieved introducing a new compartment denoted by S_R , which stands for susceptible after recovery, see ²⁸. Our final model reads as follows:

$$\begin{cases} \dot{S} = -\frac{S}{N} \int_{\mathbb{R}} \beta(\alpha) \ dI(\alpha), \\ \dot{I} = V_{\varphi}[I(\alpha)] + \frac{S}{N} \beta(\alpha) I(\alpha) + \frac{S_{R}(\alpha)}{N} \int_{\mathbb{R}} \beta(\alpha, \hat{\alpha}) \ dI(\hat{\alpha}) - \gamma(\alpha) I(\alpha), \\ \dot{R}(\alpha) = \gamma(\alpha) \ I(\alpha) - \sigma R(\alpha), \\ \dot{S}_{R}(\alpha) = \sigma R - \frac{S_{R}(\alpha)}{N} \int_{\mathbb{R}} \beta(\alpha, \hat{\alpha}) \ dI(\hat{\alpha}), \end{cases}$$
(5.4)
$$e \ \beta(\alpha, \hat{\alpha}) \text{ is the infection rate of variant } \alpha \text{ among patients that recently (within the following particles)}$$

where $\beta(\alpha, \hat{\alpha})$ is the infection rate of variant α among patients that recently (within the last σ time period) recovered from variant $\hat{\alpha}$. The example in Figure 7 effectively constrains $\beta(\alpha, \hat{\alpha}) = 0$ for $\alpha = \hat{\alpha}$, and dampens the infection rate for all α sufficiently close to $\hat{\alpha}$. Biological information could be the driving force for such parameters, for example $\beta(\alpha, \hat{\alpha})$ could directly reflect the antigenic distance $D_{\alpha\hat{\alpha}}$ between the two variants 17,20 .

Notice that (5.4) can be interpreted as an ODE (for the compartment S), coupled with an MDE (for the compartment I), and two linear PDEs (for the compartments R and S_R). For our framework, it is convenient to interpret the two linear PDEs as MDEs. This interpretation allows to take advantage of convenient discretization schemes as explained in next section.

5.3. Approximate solutions to the ODE-MDE system

To discretize the ODE-MDE system we use the operator splitting method as follows:

Step 0. The Radon measures I, R and S_R are approximated by a finite sum of Dirac deltas centered at points of a fixed space lattice Γ of step Δx .

Step 1. We use the ODE solver to update the compartment S. Due to the approximation of the measure I, the right-hand side is a finite sum (over compact sets).

Step 2. Since the sink/source terms act as parameterized ODEs (for the parameter α), we can use the same solver to update the other compartments.

Step 3. We approximate $V_{\varphi}|_{x}$, for $x \in \Gamma$, with a finite sum of Dirac deltas centered at points of a velocity lattice Γ_v of step Δ_v . Choosing the time step so that $\Delta t \cdot \Delta v = \Delta_x$, the mass at a lattice point $x \in \Gamma$ is shifted to another point of the lattice $y \in \Gamma$, as for Lattice Approximate Solutions. We can then go back iteratively to Step 1.

5.4. Properties of the MDE-ODE SIRS model

In this section we discuss the existence of solutions for the system (5.4). More precisely rewrite the system as:

$$\dot{S} = g(S, \mu), \qquad \dot{\mu} = V[\mu] \oplus s(\mu, S), \tag{5.5}$$

where $\mu = (I, R, S_R)$ is a vector measure, $g = -\frac{S}{N} \int_{\mathbb{R}} \beta(\alpha) \ dI(\alpha)$,

$$V[\mu] = \begin{pmatrix} V_{\varphi}[I(\alpha)] \\ 0 \\ 0 \end{pmatrix},$$

and

$$s(\mu, S) = \begin{pmatrix} \frac{S}{N}\beta(\alpha)I(\alpha) + \frac{S_R(\alpha)}{N} \int_{\mathbb{R}} \tilde{\beta}(\alpha, \hat{\alpha}) \ dI(\hat{\alpha}) - \gamma(\alpha)I(\alpha) \\ \gamma(\alpha) \ I(\alpha) - \sigma R(\alpha) \\ \sigma R - \frac{S_R(\alpha)}{N} \int_{\mathbb{R}} \tilde{\beta}(\alpha, \hat{\alpha}) \ dI(\hat{\alpha}) \end{pmatrix}.$$

We have the following

Theorem 5.1. Consider the system (5.5) and assume that β , γ , $\tilde{\beta}$ are Lipschitz functions. Then the hypotheses of Theorem 4.1 are satisfied, thus there exists a Lipschitz semigroup of solutions to (5.5).

Proof. We follow the proof given in 25 for the system (5.3). The vector field g is Lipschitz continuous since β is Lipschitz continuous. The MVF V has one component given by V_{φ} and two vanishing ones, thus (H1), (H2) hold true as proved in Proposition 4.1 of 25 .

We are left to prove the estimate (4.3) for s. The source has new terms given by $\frac{S_R(\alpha)}{N} \int_{\mathbb{R}} \tilde{\beta}(\alpha, \hat{\alpha}) \ dI(\hat{\alpha})$ w.r.t. (5.3). It holds:

$$W^g\left(\frac{S^1_R(\alpha)}{N}\int_{\mathbb{R}}\tilde{\beta}(\alpha,\hat{\alpha})\ dI^1(\hat{\alpha}), \frac{S^2_R(\alpha)}{N}\int_{\mathbb{R}}\tilde{\beta}(\alpha,\hat{\alpha})\ dI^2(\hat{\alpha})\right) \leq$$

$$W^g\left(\frac{S_R^1}{N}\int_{\mathbb{R}}\tilde{\beta}\ dI^1, \frac{S_R^2}{N}\int_{\mathbb{R}}\tilde{\beta}\ dI^1\right) + W^g\left(\frac{S_R^2}{N}\int_{\mathbb{R}}\tilde{\beta}\ dI^1, \frac{S_R^2}{N}\int_{\mathbb{R}}\tilde{\beta}\ dI^2\right) = A_1 + A_2$$

Let $\tilde{S}_R^i \leq S_R^i$, i=1,2, be the measures achieving the infimum in the definition of $W^g(S_R^1,S_R^2)$ and $\pi_S \in P^{opt}(\tilde{S}_R^1,\tilde{S}_R^2)$ (the set of optimal transference plans). Then $\hat{\pi} = \int \tilde{\beta} dI^1 \pi_S$ is a transference plan between $\tilde{S}_R^1 \int \tilde{\beta} dI^1$ and $\tilde{S}_R^2 \int \tilde{\beta} dI^1$ (both well defined measures obtained by multiplying a Lipschitz function by a measure). Then we obtain:

$$A_1 \le \frac{1}{N} \int |z_1 - z_2| \, d\hat{\pi}(z_1, z_2) + \frac{1}{N} (|S_R^1 - \tilde{S}_R^1| + |S_R^2 - \tilde{S}_R^2|) \|\tilde{\beta}\|_{L^{\infty}} |I_1| \le C_1 + C_2 + C_2 + C_2 + C_3 + C_4 + C_4$$

$$\frac{1}{N} \|\tilde{\beta}\|_{L^{\infty}} |I_1| W^g(S_R^1, S_R^2).$$

Now let us pass to A_2 . Let $\tilde{I}^i \leq I^i$, i = 1, 2, be the measures achieving the infimum in the definition of $W^g(I^1, I^2)$ and $\pi_I \in P^{opt}(\tilde{I}^1, \tilde{I}^2)$ (the set of optimal transference plans). Notice that:

$$A_2 \le \frac{1}{N} |S_R^2| \cdot \left\| \int_{\mathbb{R}} \tilde{\beta} \ d(I^1 - I^2) \right\|_{L^{\infty}}.$$

To estimate the right-hand side, we first notice that:

$$\left\| \int_{\mathbb{R}} \tilde{\beta} \ d(\tilde{I}^1 - \tilde{I}^2) \right\|_{L^{\infty}} \le Lip(\tilde{\beta}) \cdot \int |z_1 - z_2| \, d\pi_I(z_1, z_2)$$

where $Lip(\tilde{\beta})$ indicates the Lipschitz constant of $\tilde{\beta}$. On the other side, for i=1,2:

$$\left\| \int_{\mathbb{R}} \tilde{\beta} \ d(I^i - \tilde{I}^i) \right\|_{L^{\infty}} \le \|\tilde{\beta}\|_{L^{\infty}} |I^i - \tilde{I}^i|.$$

Combining the last two estimates, we get:

$$A_2 \le \frac{1}{N} |S_R^2| \max\{Lip(\beta), \|\tilde{\beta}\|_{L^{\infty}}\} W^g(I^1, I^2).$$

Finally, treating the other terms as in Proposition 4.1 of ²⁵, we obtain:

$$W^g(s(\mu_1, S_1), s(\mu_2, S_2) \le M(|S_1 - S_2| + W^g(\mu_1, \mu_2))$$

and (4.3) holds true.

5.5. Simulations for MDE model

Here we visualize the time evolution of model (5.4) using simulations developed in MatLab and the discretization scheme outlined in Section 5.3. Our first simulation uses the the parameters shown in Figure 6. For all simulations, unless specified otherwise, we will consider a 60 day loss of immunity rate. In Figure 7 the simulation starts with one person infected with the variant found at the center of our variant space, and at every updating step we mutate at a maximum velocity which is dependent on the total number infected at the time, similar to what done for model (2.1). The more people there are currently infected, the faster the virus may be expected to mutate. This is modeled by adjusting the diffusion speed v as follows:

$$v = \psi \cdot \frac{1}{N} \int dI(\alpha);$$

where ψ is a chosen scale factor. The corresponding dynamics is represented in Figure 7 where the velocities grow as the total infected population grows, and will slow down if the infected population diminishes.

The symmetry in Figure 7 is due to the symmetry in the replication rates shown in Figure 6. However, infection rates may well happen to be asymmetric w.r.t. to the initial variant. Asymmetry can be represented simply by changing the replication rates, using a function that is no longer symmetrical over the center variant. In Figure 8 we exemplify this using a simple linear function as our replication rates. The resulting dynamics in Figure 9 show that the virus is "favoring" the direction of higher infection rate. Lastly, we explore loss of immunity, expanding from 60 days to 120 in Figure 10. Notice that in Figure 10 we observe a wave-like pattern in the dynamics very similar to the wave-like pattern of COVID-19, suggesting that 60 days may be too short to consider as the average time of reinfectability.

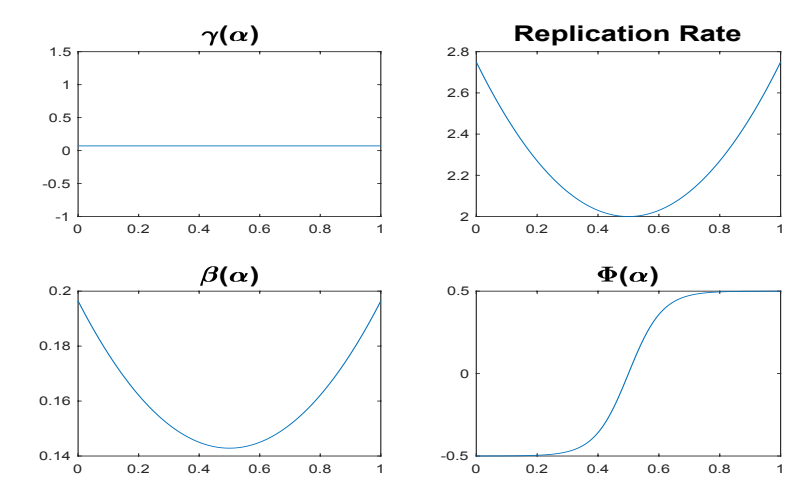


Fig. 6: Model parameters as function of variants. Top left: recovery rate, top right: replication rate, bottom left: infection rate, bottom right: mutation rate

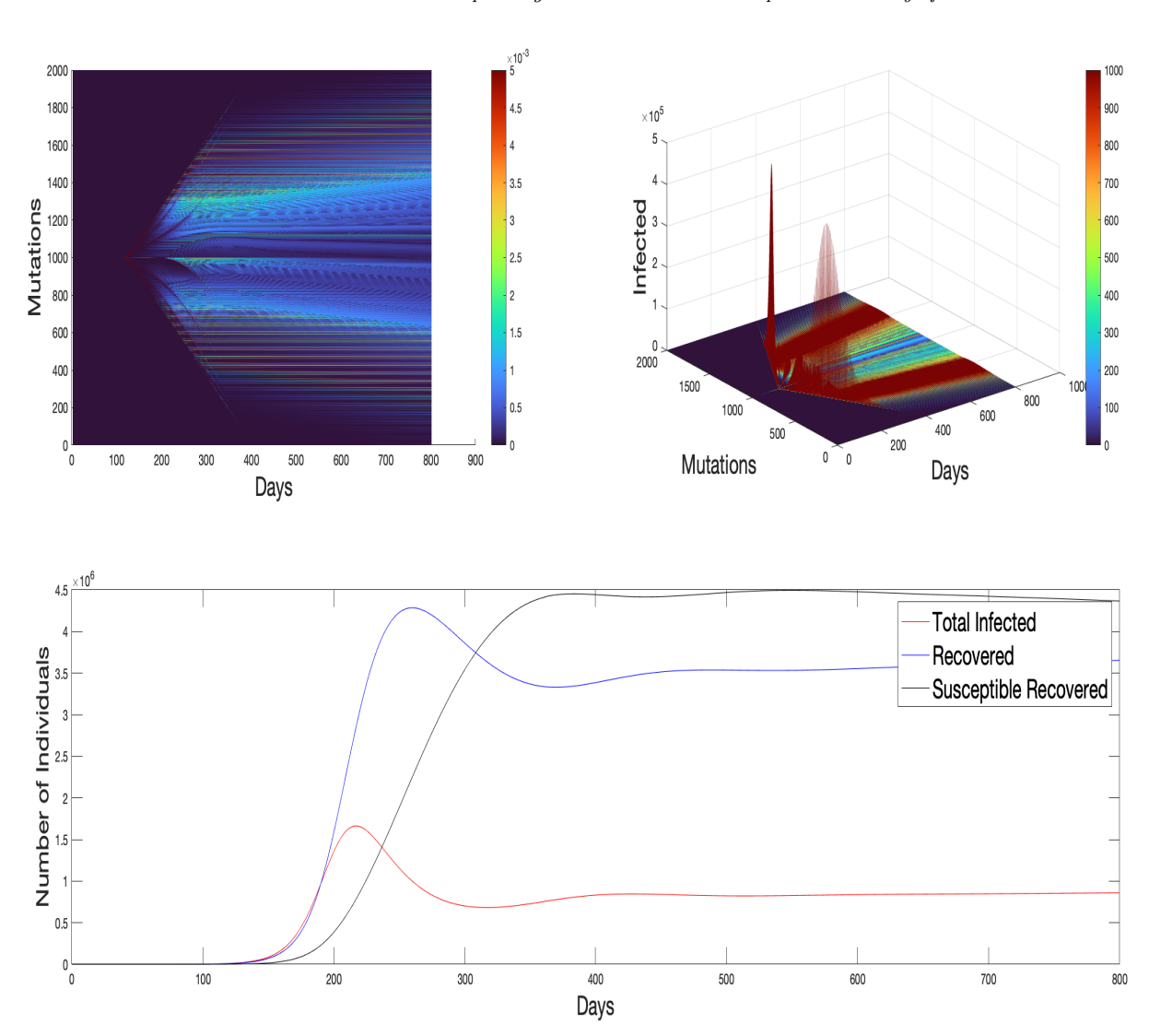


Fig. 7: Top left: heat map of infected over the variant space. Top right: Infected dynamics over time. Bottom: Dynamics of SIR model.

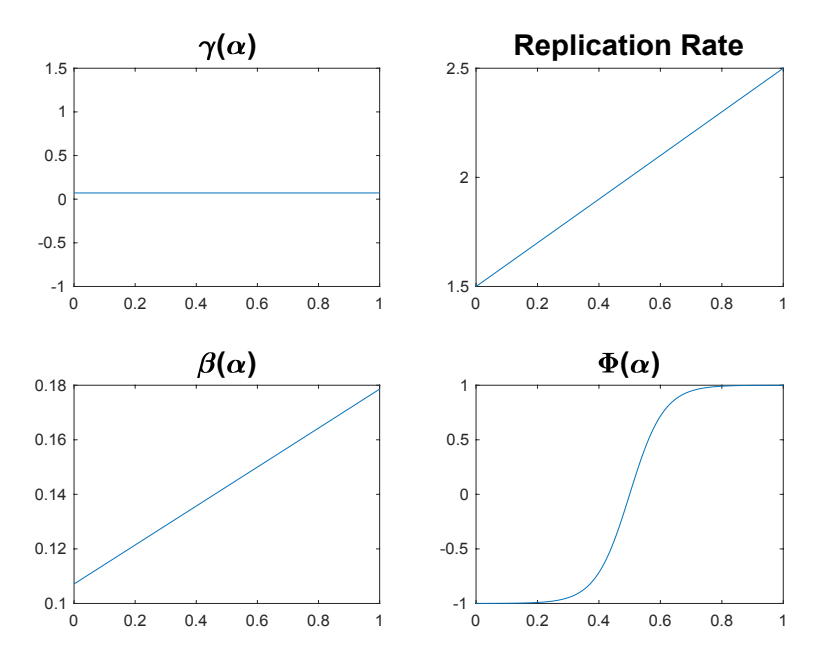


Fig. 8: Parameters with asymmetric replication rates.

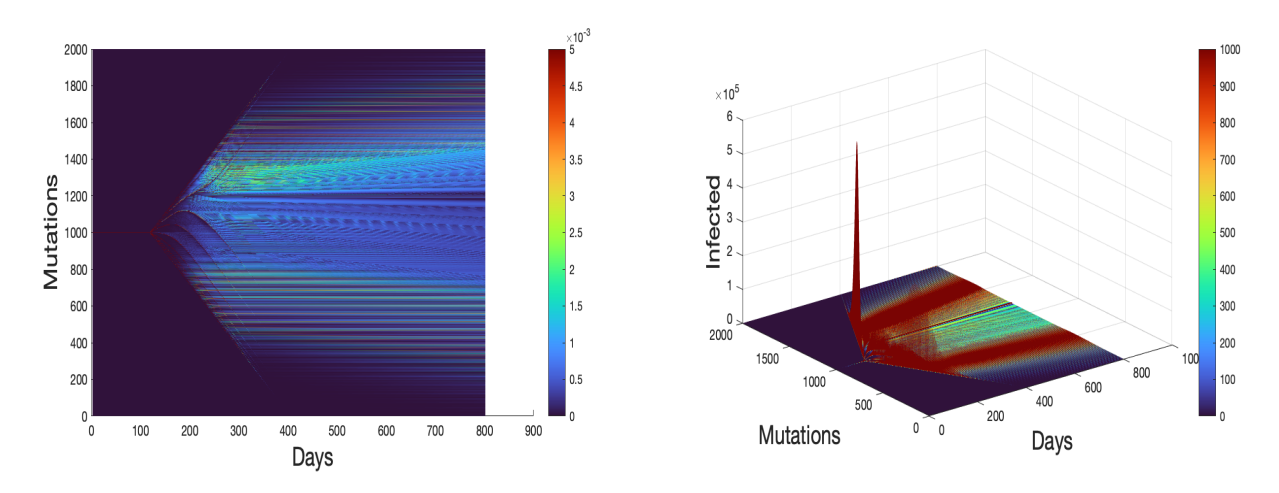


Fig. 9: Time evolution for asymmetric replication rates. Top left: heat map of infected over the variant space. Top right: Infected dynamics over time.

Mutations 1000 800

600

400 200

400

Days

200

800

1200

1000

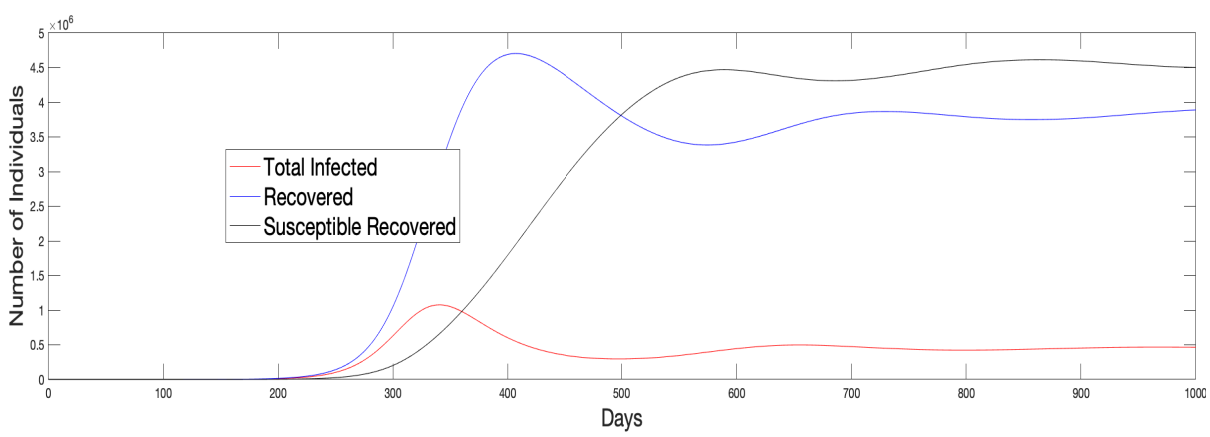


Fig. 10: Time evolution for loss of immunity after 120 days. Top left: heat map of infected over the variant space. Top right: Infected dynamics over time. Bottom: Dynamics of SIR model.

Acknowledgements

The authors would like to acknowledge the support of the NSF CMMI project # 2033580 "Managing pandemic by managing mobility" in collaboration with Cornell University and Vanderbilt University, and the support of the Joseph and Loretta Lopez Chair endowment.

References

- S. R. Allred, S. T. McQuade, N. J. Merrill, B. Piccoli, D. Spielman, C. Villacis, R. Whiting, A. Yadav, D. Zacher, and D. Ziminski. Regional health system shortfalls with a novel covid-19 model. 2020.
- N. Bellomo, R. Bingham, M. Chaplain, G. Dosi, G. Forni, D. A. Knopoff, J. Lowengrub, R. Twarock, and M.E. Virgillito. A multiscale model of virus pandemic: Heterogeneous interactive entities in a globally connected world. *Mathematical Models and Methods in Applied Sciences*, 30(08):1591–1651, 2020.
- 3. N. Bellomo, D. Burini, and N. Outada. Multiscale models of covid-19 with mutations and variants. *Networks and Heterogeneous Media*, 17(3):293–310, 2022.
- P. Block, M. Hoffman, I. J. Raabe, J.B. Dowd, C. Rahal, R. Kashyap, and M. C. Mills. Social network-based distancing strategies to flatten the covid-19 curve in a post-lockdown world. *Nature Human Behaviour*, 4(6):588–596, 2020.
- R. K. Borchering, C. Viboud, E. Howerton, C. P. Smith, S. Truelove, M. C. Runge, N. G. Reich, L. Contamin, J. Levander, J. Salerno, et al. Modeling of future covid-19 cases, hospitalizations, and deaths, by vaccination rates and nonpharmaceutical intervention scenarios—united states, april—september 2021. Morbidity and Mortality Weekly Report, 70(19):719, 2021.
- T. Britton, F. Ball, and P. Trapman. A mathematical model reveals the influence of population heterogeneity on herd immunity to sars-cov-2. *Science*, 369(6505):846–849, 2020.
- F. Camilli, G. Cavagnari, R. De Maio, and B. Piccoli. Superposition principle and schemes for measure differential equations. *Kinetic and Related Models*, 14(1):89–113, 2021.
- 8. T. Carvalho, F. Krammer, and A. Iwasaki. The first 12 months of covid-19: a timeline of immunological insights. *Nature Reviews Immunology*, 21(4):245–256, 2021.
- 9. M. Catak and N. Duran. Nonlinear markov chain modelling of the novel coronavirus (covid-19) pandemic. *medRxiv*, 2020.
- Y. C. Chen, P.E. Lu, C. S. Chang, and T. H. Liu. A time-dependent SIR model for COVID-19 with undetectable infected persons. *IEEE Transactions on Network* Science and Engineering, 7(4):3279–3294, 2020.
- 11. M. Chyba, R. M. Colombo, M. Garavello, and B. Piccoli. Advanced mathematical methodologies to contrast covid-19 pandemic. *Networks and Heterogeneous Media*, 17(3):i–ii, 2022.
- 12. B. J. Coburn, B. G. Wagner, and S. Blower. Modeling influenza epidemics and pandemics: insights into the future of swine flu (h1n1). *BMC medicine*, 7(1):1–8, 2009.
- 13. R. M. Colombo and M. Garavello. Well posedness and control in a nonlocal sir model. *Applied Mathematics & Optimization*, 84(1):737–771, 2021.
- 14. R. M. Colombo, M. Garavello, Francesca Marcellini, and Elena Rossi. An age and space structured SIR model describing the Covid-19 pandemic. *Journal of mathematics in industry*, 10:Paper No. 22, 20, 2020.
- 15. O. Dalgıç, O. Ozaltın, W. A. Ciccotelli, and F. S. Erenay. Deriving effective vaccine

- allocation strategies for pandemic influenza: Comparison of an agent-based simulation and a compartmental model. PloS one, 12(2):e0172261, 2017.
- 16. R. de M. R. Rafael, M. Neto, M. M. B. de A. D. Carvalho, HMSL. David, S. Acioli, and M.G. de A. Faria. Epidemiology, public policies and covid-19 pandemics in brazil: what can we expect. Rev enferm UERJ, 28:e49570, 2020.
- 17. W. Dejnirattisai, J. Huo, D. Zhou, J. Zahradník, P. Supasa, C. Liu, H. M. E. Duyvesteyn, H. M. Ginn, A. J. Mentzer, A. Tuekprakhon, et al. Sars-cov-2 omicron-b. 1.1. 529 leads to widespread escape from neutralizing antibody responses. Cell, 2022.
- 18. D.Kim and A. Quaini. Coupling kinetic theory approaches for pedestrian dynamics and disease contagion in a confined environment. Mathematical Models and Methods in Applied Sciences, 30(10):1893-1915, 2020.
- 19. K. Dooling, N. McClung, M. Chamberland, M. Marin, M. Wallace, B. P. Bell, G. M. Lee, H. K. Talbot, J. R. Romero, and S. E. Oliver. The advisory committee on immunization practices' interim recommendation for allocating initial supplies of covid-19 vaccine—united states, 2020. Morbidity and Mortality Weekly Report, 69(49):1857, 2020.
- 20. A. Dubey, S. Choudhary, P. Kumar, and S. Tomar. Emerging sars-cov-2 variants: Genetic variability and clinical implications. Current microbiology, 79:20, December
- 21. D. J. D. Earn, J. Dushoff, and S. A. Levin. Ecology and evolution of the flu. Trends in ecology & evolution, 17(7):334-340, 2002.
- 22. L. Espenhain, T. Funk, M. Overvad, S. M. Edslev, J. Fonager, A. C. Ingham, et al. Epidemiological characterisation of the first 785 sars-cov-2 omicron variant cases in denmark, december 2021. Eurosurveillance, 26(50):2101146, 2021.
- 23. E. Lavezzo et al. Suppression of a sars-cov-2 outbreak in the italian municipality of vo'. Nature, 584(7821):425-429, 2020.
- 24. G. Giordano, F. Blanchini, and R. et al. Bruno. Modelling the covid-19 epidemic and implementation of population-wide interventions in italy. Nature Medicine, 2020.
- X. Gong and B. Piccoli. A measure model for the spread of viral infections with mutations. Networks and Heterogeneous Media, 17(3):427-, 2022.
- I. Gordo, M. G. M. Gomes, D. G. Reis, and P. Campos. Genetic diversity in the sir model of pathogen evolution. PloS one, 4(3):e4876, 2009.
- N. Hoertel, M. Blachier, F. Limosin, M. Sanchez-Rico, C. Blanco, M. Olfson, S. Luchini, M. Schwarzinger, and H. Leleu. Optimizing sars-cov-2 vaccination strategies in france: Results from a stochastic agent-based model. medRxiv, 2021.
- J. Hu, C. Li, S. Wang, T. Li, and H. Zhang. Genetic variants are identified to increase risk of covid-19 related mortality from uk biobank data. Human genomics, 15(1):1-10, 2021.
- 29. V. Kala, K. Guo, E. Swantek, A. Tong, M., Chyba, Y. Mileyko, C. Gray, T. Lee, and A. E. Koniges. Pandemics in hawaii: 1918 influenza and covid-19. In The Ninth International Conference on Global Health Challenges GLOBAL HEALTH 2020. IARIA,
- 30. A. B. O. Kaltoum. Mutations and polymorphisms in genes involved in the infections by covid 19: a review. *Gene reports*, 23:101062, 2021.
- 31. S. S. A. Karim and Q. A. Karim. Omicron sars-cov-2 variant: a new chapter in the covid-19 pandemic. The Lancet, 398(10317):2126-2128, 2021.
- 32. W. O. Kermack and A. G. McKendrick. Contributions to the mathematical theory of epidemics. ii.—the problem of endemicity. Proceedings of the Royal Society of London. Series A, containing papers of a mathematical and physical character, 138(834):55–83, 1932.

- 22 R. Weightman, A. Sbarra, B. Piccoli
- P. Kunwar, O. Markovichenko, M. Chyba, Y. Mileyko, A. Koniges, and T. Lee. A study of computational and conceptual complexities of compartment and agent based models. arXiv preprint arXiv:2108.11546, 2021.
- 34. K. Kupferschmidt. Evolving threat, 2021.
- 35. K. O. Kwok, F. Lai, W. I. Wei, S. Y. S. Wong, and J. W. T. Tang. Herd immunity—estimating the level required to halt the covid-19 epidemics in affected countries. *Journal of Infection*, 80(6):e32–e33, 2020.
- 36. A. T. Levin, W. P. Hanage, N. Owusu-Boaitey, K. B. Cochran, S. P. Walsh, and G. Meyerowitz-Katz. Assessing the age specificity of infection fatality rates for covid-19: systematic review, meta-analysis, and public policy implications. *European journal* of epidemiology, 35(12):1123–1138, 2020.
- 37. H. Li, L. Wang, M. Zhang, Y. Lu, and W. Wang. Effects of vaccination and non-pharmaceutical interventions and their lag times on the covid-19 pandemic: Comparison of eight countries. *PLoS neglected tropical diseases*, 16(1):e0010101, 2022.
- 38. H. Liu, J. Zhang, J. Cai, X. Deng, C. Peng, X. Chen, J. Yang, Q. Wu, Z. Chen, W. Zheng, et al. Herd immunity induced by covid-19 vaccination programs to suppress epidemics caused by sars-cov-2 wild type and variants in china. *medRxiv*, 2021.
- Q. Luo, R. Weightman, S. T. McQuade, M. Díaz, E. Trélat, W. Barbour, D. Work, S. Samaranayake, and B. Piccoli. Optimization of vaccination for covid-19 in the midst of a pandemic. Networks and Heterogeneous Media, 17:443

 –466, 2022.
- 40. L. Matrajt, J. Eaton, T. Leung, and E. R. Brown. Vaccine optimization for covid-19: Who to vaccinate first? *Science Advances*, 7(6):eabf1374, 2021.
- S. T. McQuade, R. Weightman, N.J. Merrill, A. Yadav, E. Trélat, S. R. Allred, and B. Piccoli. Control of covid-19 outbreak using an extended seir model. *Mathematical Models and Methods in Applied Sciences*, 31(12):2399–2424, 2021.
- 42. A. Muniyappan, B. Sundarappan, P. Manoharan, M. Hamdi, K. Raahemifar, S. Bourouis, and V. Varadarajan. Stability and numerical solutions of second wave mathematical modeling on covid-19 and omicron outbreak strategy of pandemic: Analytical and error analysis of approximate series solutions by using hpm. *Mathematics*, 10(3):343, 2022.
- 43. S Nasreen, H Chung, S He, KA Brown, JB Gubbay, SA Buchan, et al. Effectiveness of mrna and chadox1 covid-19 vaccines against symptomatic sars-cov-2 infection and severe outcomes with variants of concern in ontario. medrxiv 2021, 2021.
- 44. B. Piccoli. Measure differential equations. Archive for Rational Mechanics and Analysis, 233(3):1289–1317, 2019.
- 45. B. Piccoli and F. Rossi. Measure dynamics with probability vector fields and sources. Discrete & Continuous Dynamical Systems, 39(11):6207, 2019.
- 46. Roghani. The influence of covid-19 vaccination on daily cases, hospitalization, and death rate in tennessee, united states: Case study. *medRxiv*, 2021.
- N. W. Ruktanonchai, JR.Floyd, S. Lai, C. W. Ruktanonchai, A. Sadilek, P. Rente-Lourenco, X. Ben, A. Carioli, J. Gwinn, JE. Steele, et al. Assessing the impact of coordinated covid-19 exit strategies across europe. *Science*, 369(6510):1465–1470, 2020.
- 48. M. Shaker, E. M. Abrams, and M. Greenhawt. A cost-effectiveness evaluation of hospitalizations, fatalities, and economic outcomes associated with universal versus anaphylaxis risk-stratified covid-19 vaccination strategies. *The Journal of Allergy and Clinical Immunology: In Practice*, 2021.
- 49. P. Webster. Covid-19 timeline of events. Nature medicine, 27(12):2054–2055, 2021.
- 50. Z. Xu, H. Zhang, and Z. Huang. A continuous markov-chain model for the simulation of covid-19 epidemic dynamics. *Biology*, 11(2):190, 2022.
- 51. F. Yu, L. Lau, M. Fok, J. Lau, and K. Zhang. Covid-19 delta variants—current status

and implications as of august 2021. Precision Clinical Medicine, 4(4):287–292, 2021. 52. J. Zhang, M. Litvinova, Y. Liang, Y. Wang, W. Wang, S. Zhao, Q. Wu, S. Merler, C. Viboud, A. Vespignani, et al. Changes in contact patterns shape the dynamics of the covid-19 outbreak in china. Science, 368(6498):1481-1486, 2020.